the upwelling radiation at all levels in the deep interior of a cloud. In the near-infrared, on the other hand, the increased optical thickness leads to a reduction in the upwelling radiance in the middle of a cloud at wavelengths where the absorption of solar radiation by water droplets is significant.
13. For typical maritime conditions, the droplet concentration is $N \propto C^{0.8}$, where C is the CCN concentration at 1% supersaturation. Thus an increase of 80 drops per cubic centimeter would require approximately 240 CCN per cubic centimeter, which is consistent with the measurements in Fig. 3C; see S. Twomey, *J. Phys. Chem.* **84**, 1459 (1980).
14. L. F. Radke, S. K. Domonkos, P. V. Hobbs, *J. Rech. Atmos.* **15**, 225 (1981).
15. J. Hallet and J. Hudson, *Aerosol Sci. Technol.* **10**, 70 (1989).
16. P. V. Hobbs, J. L. Stith, L. F. Radke, *J. Appl. Meteorol.* **19**, 439 (1980); R. F. Pueschel, E. W. Barrett, D. L. Wellman, J. A. McGuire, *Geophys. Res. Lett.* **8**, 221 (1981).
17. L. F. Radke, J. H. Lyons, P. V. Hobbs, J. A. Coakley, *Proceedings of the 10th International Cloud Physics Conference*, Bad Homburg, Federal Republic of Germany, 15 to 20 August 1988 (Deutscher Wetterdienst, Offenbach am Main, FRG, 1988), pp. 121–123; W. M. Porch, C. J. Kao, T. G. Kyle, R. G. Kelley, in *Symposium on the Role of Clouds in Atmospheric Chemistry and Global Climate*, Anaheim, CA, 30 January to 3 February 1989 (American Meteorological Society, Boston, 1989), pp. 161–164.
18. B. A. Albrecht, *Science* **245**, 1227 (1989).
19. We thank P. V. Hobbs, P. A. Durkee, J. H. Lyons, and H. Terry for useful comments and contributions. The coordinating role of the FIRE science team is gratefully acknowledged. This work was supported in part by National Science Foundation grant ATM-8615344 (L.F.R. and M.D.K.) and National Aeronautics and Space Administration grant NAG-1-935 (J.A.C.)

26 June 1989; accepted 2 October 1989

Structure of Complex of Synthetic HIV-1 Protease with a Substrate-Based Inhibitor at 2.3 Å Resolution

MARIA MILLER, JENS SCHNEIDER, BANGALORE K. SATHYANARAYANA, MIHALY V. TOTH, GARLAND R. MARSHALL, LEIGH CLAWSON, LINDA SELK, STEPHEN B. H. KENT,*† ALEXANDER WLODAWER†

The structure of a complex between a peptide inhibitor with the sequence *N*-acetyl-Thr-Ile-Nle-Ψ[CH_2-NH]-Nle-Gln-Arg.amide (Nle, norleucine) with chemically synthesized HIV-1 (human immunodeficiency virus 1) protease was determined at 2.3 Å resolution (*R* factor of 0.176). Despite the symmetric nature of the unliganded enzyme, the asymmetric inhibitor lies in a single orientation and makes extensive interactions at the interface between the two subunits of the homodimeric protein. Compared with the unliganded enzyme, the protein molecule underwent substantial changes, particularly in an extended region corresponding to the "flaps" (residues 35 to 57 in each chain), where backbone movements as large as 7 Å are observed.

RETROVIRAL PROTEASES, WHICH are members of the aspartic protease family, specifically process high molecular weight viral polyproteins into individual structural proteins and enzymes (*1*). Mutation of the active site Asp to Asn in HIV-1 protease (HIV-1 PR) prevents processing of polyprotein (*2*), so that immature, noninfective virions result. Thus specific inhibitors of HIV-1 PR would serve as candidates for AIDS therapeutics.

The structure of cloned HIV-1 PR has been determined at 3 Å (*3*). Important corrections were made in a 2.8 Å x-ray study with synthetic HIV-1 PR (*4*) and have been confirmed for the cloned material (*5*). More detailed information needed for inhibitor design can be gleaned from studies of enzymes complexed with substrate-derived inhibitors. For cellular aspartic proteases, extensive investigation of inhibitor complexes with endothiapepsin (*6*), rhizopuspepsin (*7*), and penicillopepsin (*8*) have been reported.

Modeling of the interaction of inhibitors and substrates with HIV-1 PR (*9*) could only make limited predictions in the absence of experimental data, and the available crystal form of the HIV-1 PR was not suitable for inhibitor studies because of the presence of only one subunit (one-half of the molecule) in the asymmetric unit and the limited diffraction (*3–5*). For these reasons we cocrystallized HIV-1 PR with a substrate-based inhibitor.

An inhibitor was designed based on the sequence of a good peptide substrate for the enzyme. Hexapeptides derived from known cleavage sites of the viral *gag-pol* polyprotein products were synthesized, and several were shown to be substrates (*10*). The hexapeptide substrate with the lowest Michaelis constant K_m (1.4 m*M*), Ac-Thr-Ile-Met-Met-Gln-Arg.amide (where the amide is on the carboxyl terminus), was chosen as a candidate for further modification. The isosteric amino acid norleucine (Nle), in which the sulfur of the Met side chain is replaced by a methylene group, was used for synthetic simplification and shown to give a substrate, Ac-Thr-Ile-Nle-Nle-Gln-Arg.amide, with comparable affinity. In an approach analogous to that of Szelke *et al.* (*11*) for human renin, we prepared an inhibition of HIV-1 PR, compound MVT-101, with the sequence *N*-acetyl-Thr-Ile-Nle-Ψ[CH_2-NH]-Nle-Gln-Arg.amide (*12*), where the scissile peptide bond has been replaced by a reduced analog (*13,14*).

The crystal structure of the complex was solved by molecular replacement using the native HIV-1 PR (*4*) as a starting model (*15*). The $|F_o - F_c|\alpha_c$ map based on the phases from the preliminary refinement showed density in the active site corresponding to the inhibitor. A model of the hexapeptide with a reduced peptide bond was fitted easily, with the polarity indicated primarily by the bulky side chain of Arg^{206}. The positions of all six residues of the inhibitor are well defined by the electron density (Fig. 1). The inhibitor binds to the

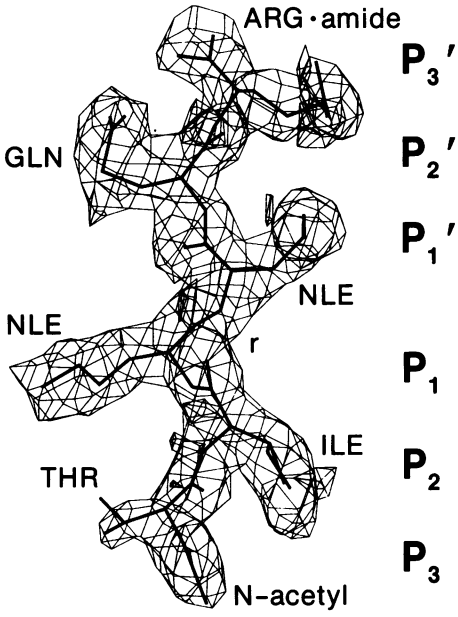

Fig. 1. A view of the electron density and of the final atomic model of the inhibitor MVT-101. This $|2F_o - F_c|\alpha_c$ electron density map was calculated after refinement and was contoured at the 0.8σ level. All of the atoms belonging to the inhibitor molecule, with the exception of Cγ of Thr^{201}, are in the density.

M. Miller, B. K. Sathyanarayana, A. Wlodawer, Crystallography Laboratory, NCI–Frederick Cancer Research Facility, BRI-Basic Research Program, P.O. Box B, Frederick, MD 21701.
J. Schneider, L. Clawson, L. Selk, S. B. H. Kent, Division of Biology, California Institute of Technology, Pasadena, CA 91125.
M. V. Toth and G. R. Marshall, Department of Pharmacology, Washington University School of Medicine, St. Louis, MO 63110.

*Current address: Graduate School of Science and Technology, Bond University, Queensland, Australia 4229.
†To whom correspondence should be addressed.

active site of the protease in an extended conformation (Table 1). The reduced peptide bond between the two Nle residues deviates from planarity by 38°—a value similar to that reported for the reduced peptide inhibitor of rhizopuspepsin (7). The inhibitor molecule makes extensive interactions with the enzyme at the interface between the protein subunits. It is more than 80% excluded from contact with the surrounding solvent by the protein molecule, with only the amino- and carboxyl-terminal amino acids partially exposed.

Six direct inhibitor-enzyme hydrogen bonds between the main chain O and N atoms involve Asp^{29} N, Gly^{27} O, and Gly^{48} O from both monomers (Fig. 2). The flaps (Ile^{50} N) bind through a water bridge to carbonyls of inhibitor residues in the P2 and P1′ subsites. The side chain carboxyl of Asp^{29} forms a long hydrogen bond with the nitrogen of the *N*-acetyl terminus, while the carboxyl of $Asp^{29'}$ (primes indicate the second subunit) interacts with the inhibitor carboxyl-terminus amide group. Two water molecules are hydrogen-bonded to the amido carbonyls of the end groups of the reduced peptide. Specific hydrogen-bonded interactions with the main chain of the inhibitor in P1-P2 and P1′-P2′ are made by the carbonyl oxygens of Gly^{27} and $Gly^{27'}$, as predicted (*5, 9*). This interaction necessitated the rotation of the planes of the carbonyls of the Gly^{27} and $Gly^{27'}$ peptide groups by almost 90° compared with the native structure.

Extensive van der Waals contacts with the enzyme residues define the binding pockets of the complex (Fig. 3 and Table 2). Side chains P2, P1, P1′, and P2′ are located in well-defined hydrophobic pockets. However, Arg^{206} is held at S3′ by ionic interactions with the carboxylate of $Asp^{29'}$, while Thr^{201} at S3 does not seem to interact strongly with the enzyme and its side chain appears to be disordered (Fig. 1).

Binding of the inhibitor introduces substantial conformational changes to the enzyme (Fig. 4). The overall movement of the subunits can be described as a hinge motion by 1.7°, with the hinge axis located in the intersubunit β-sheet interface (the rotation axis is perpendicular to the view shown in Fig. 3). This motion slightly tightens the cavity of the active site, but the major rearrangement of that area involves very large motion of the flap regions. This motion is significant for as much as a quarter of each subunit, since all Cα atoms for residues 34 to 57 in either flap shift by more than 1 Å, with the movement as large as 7 Å for the tips of the flaps (around residue 50). The movement of both flaps is grossly symmetric, with maximum deviation of less than 1 Å between equivalent Cα atoms. The major asymmetric element lies in the tip of the flap and is introduced by the flip of a peptide bond between residues 50′ and 51′ compared with their counterparts in the other molecule. Only one hydrogen bond (N51 · · · O50′) connects these polypeptide chains, whereas N51′ and O50 hydrogen-bond to water molecules only.

A topological change occurs between the arrangements of the tips of the flaps in the native and inhibited HIV-1 PR (Fig. 4). The flap of the bottom subunit in the native enzyme is above the one from the top

Table 1. The backbone didhedral angles of the substrate-derived inhibitor in the enzyme-inhibitor complex. These angles correspond to an extended conformation of the polypeptide.

Residue	Angle (degree)		
	φ	ψ	ω
Thr^{201}		125	−176
Ile^{202}	−121	92	−178
Nle^{203}	−92	72*	142*
Nle^{204}	−92*	154	−179
Gln^{205}	−151	123	178
Arg^{205}	−81	129	

*Reduced peptide bond.

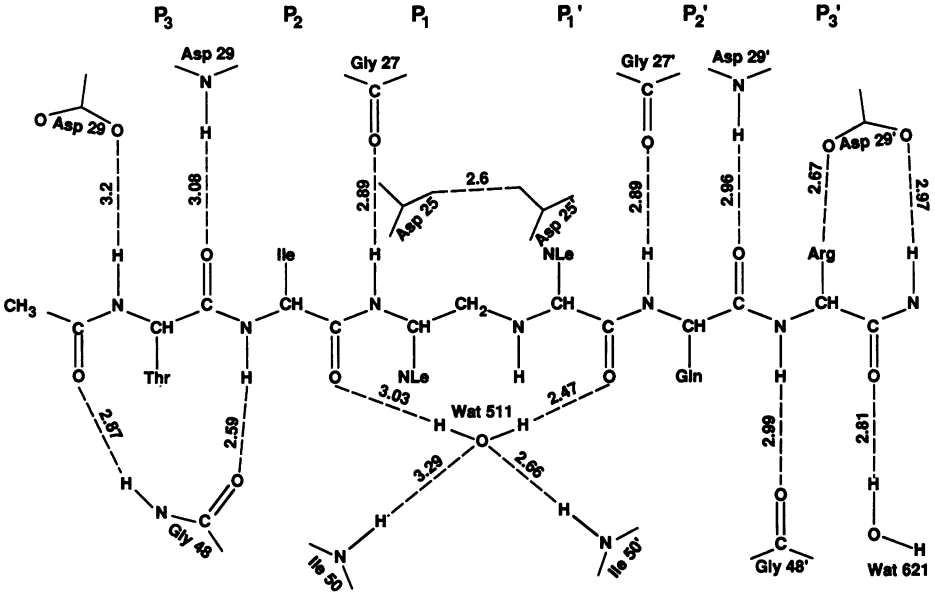

Fig. 2. Schematic representation of the hydrogen bond interactions between the inhibitor and the protein. The distances marked are between nonhydrogen atoms.

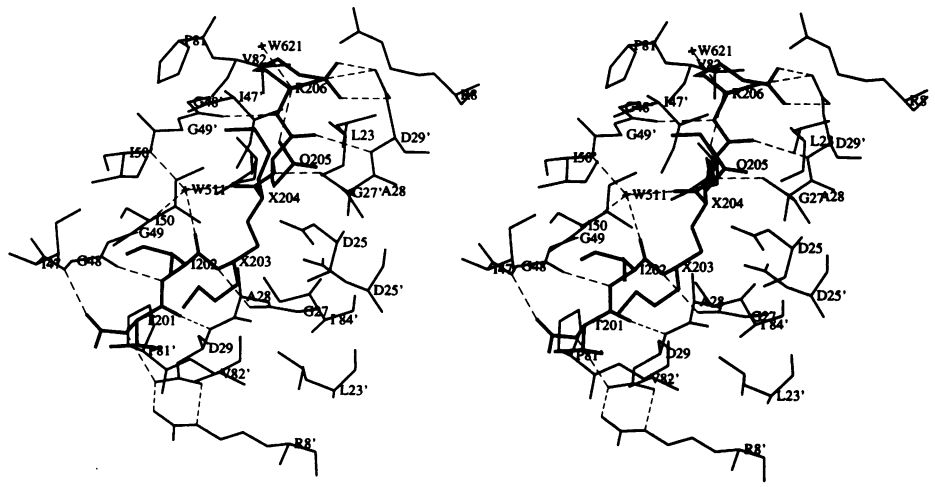

Fig. 3. The binding of MVT-101 to the active site of HIV-1 PR. The inhibitor is shown in thick lines. Only those residues of the enzyme less than 4.2 Å from the inhibitor are shown in thinner lines. Hydrogen bonds are dashed (*17*). Specific recognition of substrate or inhibitor appears to arise from complementary interactions between side chains of the inhibitor and pockets on the enzyme that involve at least six residues of the inhibitor in the extended conformation. As discussed in the text, specific ionic interactions occur within protease molecule at S3 and between the substrate carboxyl terminal Arg and $Asp^{29'}$ in S3′.

subunit, whereas the opposite is true for the inhibited enzyme. The flaps may rearrange themselves after opening to allow the inhibitor to enter the binding cleft. The arrangement of the flaps in the native enzyme may also be an artifact of crystal packing, since the tips of the flaps are involved in intermolecular contacts (*3, 4*).

Binding of the inhibitor leads to substantial movement in residues 77 to 82 in both subunits. The maximum shifts in the Cα positions in that region exceed 2 Å, and the direction of movement also decreases the size of the active site cavity. The driving force for this motion is a hydrophobic interaction in both subunits of Pro^{81} and Val^{82} with the Nle residues (inhibitor subsites P1 and P1′); moreover, it is consistent with the movement of the hinge region of the flaps, which is immediately adjacent. This motion was not predicted in model building (*5, 9*).

Local asymmetry is also introduced as a consequence of different residues occupying the sites P3 and P3′. In the native enzyme Asp^{29} forms ionic interactions with $Arg^{8'}$ and Arg^{87}. This interaction remains identical in one of the monomers, but $Arg^{8'}$ is pushed away by Arg^{206} of the inhibitor, which replaces it as the partner of $Asp^{29'}$ in the salt bridge. A bidentate ion pair between the carboxylate of $Asp^{29'}$ and the guanidinium group of Arg^{206} (Fig. 3) may explain why the Lys^{206} analog is a poor inhibitor (*16*). As a result of all these effects, the two subunits forming the dimer, which were crystallographically identical in the native structure, deviate in the complex by 0.4 Å (root-mean-square Cα deviations). The long axis of the protease (vertical in Fig. 4) is aligned with the *x*-axis of the unit cell, and large solvent channels are parallel to this axis. Both ends of the inhibitor face these channels and are not involved in crystal contacts, so that even inhibitors longer than the hexapeptide-based one we have described may be accommodated.

The data reported here should lead to a better understanding of the details of inhibitor-enzyme interactions, which will be useful in determining the molecular origin of substrate specificity and in the design of HIV-1 PR inhibitors. Such inhibitors have potential as AIDS therapeutics.

Table 2. Contacts between HIV-1 PR dimer and the substrate-derived inhibitor. The binding pocket is defined as those residues of the protein that are within 4.2 Å radius of the inhibitor (*6*). Underlined residues have moved by more than 2 Å (at Cα) as a result of inhibitor binding.

Subsite (inhibitor)	Binding pockets (enzyme)
P3: Thr^{201}	S3: $Arg^{8'}$, Asp^{29}, $\underline{Gly^{48}}$
P2: Ile^{202}	S2: Ala^{28}, $\underline{Ile^{47}}$, $\underline{Ile^{50'}}$, Ile^{84}
P1: Nle^{203}	S1: $Leu^{23'}$, $Asp^{25'}$, $\underline{Ile^{50}}$, $\underline{Pro^{81'}}$, $\underline{Val^{82'}}$ $Ile^{84'}$
P1′: Nle^{204}	S1′: $Leu^{23'}$, Gly^{27}, Asp^{25}, $\underline{Ile^{50'}}$, $\underline{Pro^{81}}$, $\underline{Val^{82}}$, Ile^{84}
P2′: Gln^{205}	S2′: $Val^{32'}$, $\underline{Ile^{47'}}$, $\underline{Gly^{48'}}$, $\underline{Ile^{50}}$
P3′: Arg^{206}	S3′: Arg^{8}, $Gly^{27'}$, $Asp^{29'}$, $\underline{Gly^{48'}}$, Val^{82}

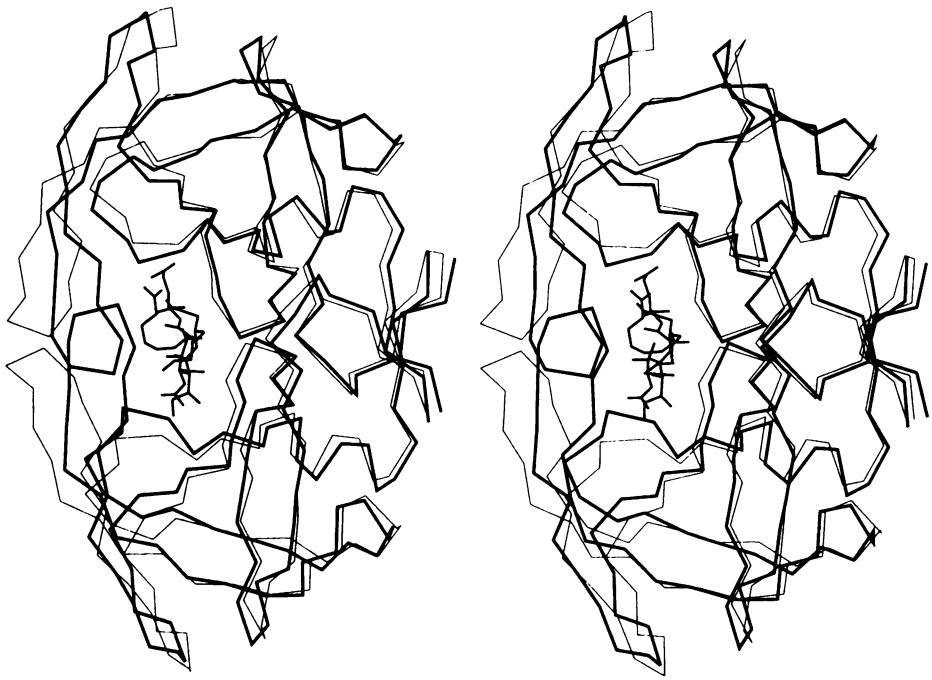

Fig. 4. Stereo tracing of the superimposed Cα backbones of the native (thin lines) and inhibited (thick lines) protease dimers, with the inhibitor as reported here marked in medium lines. The large movements of the flap regions, as well as the loop containing residues 79 to 82, can be clearly seen. The full set of atomic parameters for this model, including both main chain and side chain atoms, has been deposited with the Brookhaven Protein Data Bank (set 4HVP).

REFERENCES AND NOTES

1. H.-G. Kräusslich and E. Wimmer, *Annu. Rev. Biochem.* **57**, 701 (1988).
2. S. Seelmeier, H. Schmidt, V. Turk, K. von der Helm, *Proc. Natl. Acad. Sci. U.S.A.* **85**, 6612 (1988); J. Mous, E. P. Heimer, S. F. J. LeGrice, *J. Virol.* **62**, 1433 (1988).
3. M. A. Navia *et al.*, *Nature* **337**, 615 (1989).
4. A. Wlodawer *et al.*, *Science* **245**, 616 (1989).
5. R. Lapatto *et al.*, *Nature* , in press.
6. A. Sali *et al.*, *EMBO J.* **8**, 2179 (1989).
7. K. Suguna, E. A. Padlan, C. W. Smith, W. D. Carlson, D. R. Davies, *Proc. Natl. Acad. Sci. U.S.A.* **84**, 7009 (1987).
8. M. N. G. James and A. R. Sielecki, in *Biological Macromolecules and Assemblies*, F. A. Jurnak and A. McPherson, Ed. (Wiley, New York, 1987), vol. 3, pp. 413–482.
9. I. T. Weber *et al.*, *Science* **243**, 928 (1989).
10. M. V. Toth, F. Chin, L. Clawson, L. Selk, S. B. H. Kent, G. R. Marshall, unpublished results.
11. M. Szelke *et al.*, *Nature* **229**, 555 (1982).
12. The dipeptide analog, Nle-Ψ[CH_2NH]-Nle was prepared in situ by reductive alkylation during solid-phase peptide synthesis. Four equivalents of tBoc-Nle (*tert*-butyloxycarbonyl) aldehyde prepared by the procedure of J. A. Fehrentz and B. Castro [*Synthesis* **8**, 676 (1983)] in *N,N*-dimethylformamide containing 1% acetic acid was reacted with the trifluoroacetate salt of the peptide amine resin, Nle-Gln-Arg-*p*-methylbenzhydrylamine polymer, followed by reduction with four equivalents of $NaCNBH_3$ in portions according to Y. Sasaki *et al.* [*J. Med. Chem.* **30**, 1162 (1987)]. Additions of Boc-Ile, and Boc-Thr(OBzl) (benzyl-protected carbonyl), followed by acetylation of the amino terminal and by cleavage from the polymeric support with hydrofluoric acid afforded MVT-101, which was purified by reversed-phase high-performance liquid chromatography. The inhibition constant K_I for MVT-101 was 0.78 μ*M*.
13. HIV-1 PR was prepared by total chemical synthesis as previously described (*4, 14*). Enzyme and inhibitor (20-fold excess) were cocrystallized at *p*H 5.4. The synthetic enzyme was stored in phosphate buffer, *p*H 7, in 20% glycerol at −20 °C. For inhibitor binding, enzyme was concentrated to 6 mg/ml with Centricon-10 microconcentrators, while simultaneously exchanging the buffer for 20 m*M* sodium acetate, *p*H 5.4. An MVT-101 solution (5 mg in 100 μl of dimethyl sulfoxide) was mixed with protein to yield 20-fold molar excess of the inhibitor relative to the dimer. Crystals grew at room temperature in hanging drops from 60% ammonium sulfate. They appeared within a few days as thin rods with maximum dimensions of 0.3 mm by 0.12 mm by 0.06 mm (space group, $P2_12_12_1$ with unit cell lengths $a = 51.7$, $b = 59.2$, $c = 62.45$ Å). The asymmetric unit contained two identical 99-residue polypeptide chains (forming a homodimeric enzyme molecule) and one inhibitor molecule. A crystal of the protease–MVT-101 complex was mounted in a capillary and placed on a rotating-anode diffractometer equipped with a Siemens area detector [A. J. Howard *et al.*, *J. Appl. Crystallogr.* **20**, 383 (1987)]. Data were collected for a period of 8 days from four separate orientations (95° rotation in each); 55,569 reflections measured at 2.25 Å resolution reduced to 8,740 unique data, of which 7,943 were observed

[intensity $I > 1.5\sigma(I)$]. The merging R was 0.068 and the data were complete to 2.4 Å, while more than 60% of the data in the last shell were also measured.

14. S. B. H. Kent, *Annu. Rev. Biochem.* **57**, 957 (1988); J. Schneider and S. B. H. Kent, *Cell* **54**, 363 (1988).
15. The starting model was a crystallographic dimer of HIV-1 PR with perfect twofold symmetry. Rotation function calculations with either MERLOT [P. M. D. Fitzgerald, *J. Appl. Crystallogr.* **21**, 53 (1988)] or PROTEIN [Steigemann, thesis, Technical University, Munich (1974)] were unambiguous. The final Crowther rotation angles were (−2.5°, 85.5°, 99.5°), and this peak was found in the Patterson superposition at 4.3σ level for the data in the 10 to 3 Å shell. Several translation function algorithms also yielded consistent results, with the highest peak (6.8σ using the program RVAMAP in MERLOT) corresponding to fractional unit cell translations of (0.14, 0.405, 0.48). The preliminary orientation was further optimized with rigid-body refinement in X-PLOR [A. T. Brünger, J. Kuriyan, M. Karplus, *Science* **235**, 458 (1987)]. The molecular dynamics refinement with X-PLOR, followed by restrained least-squares refinement using PROLSQ [W. A. Hendrickson, *Methods Enzymol.* **115**, 252 (1985)], lowered the R factor from 0.49 to 0.221 for the data in the 10 to 3 Å shell. This process, which did not require manual intervention, introduced shifts as large as 7 Å in the flap regions (residues 45 to 52). Although the actual positions of the flaps resulting from this refinement were incorrect, the resulting electron density was unambiguous and allowed us to retrace the polypeptide chain without any difficulty. Further refinement with PROLSQ included the inhibitor as well as a limited number of water molecules (70 at present). The tetrahedral configuration of C and N atoms of the reduced amide in the inhibitor was specifically restrained. The solvent model is not yet complete and requires further rebuilding, but that procedure should not affect the description of the enzyme-inhibitor interactions, which are well defined. The present model is characterized by an R factor of 0.176 for 7813 reflections between 10 and 2.25 Å, with the deviations from ideality of 0.019 Å for bonds, 0.014 Å for the planes, and 0.22 Å^3 for the chiral volumes.
16. M. V. Toth and G. R. Marshall, unpublished results.
17. Abbreviations: A, Ala; D, Asp; G, Gly; I, Ile; L, Leu; P, Pro; R, Arg; T, Thr; and V, Val; W is water and X is Nle.

18. We thank M. Jaskólski for advice in the initial stages of this project, D. Davies for providing us with standard groups for least-squares refinement, and L. Palmer for critical reading of the manuscript and checking of some data. The Advanced Scientific Computing Laboratory, FCRF, provided a substantial allocation of time on their CRAY X-MP supercomputer. Research sponsored in part by the National Cancer Institute, DHHS, under contract N01-C0-74101 with BRI, in part by funds from the NSF Biological Instrumentation Division to S.B.H.K., by NIH grants SM-24483 and A-127302, and by Monsanto grant 44353K to G.R.M. The contents of this publication do not necessarily reflect the views or policies of the Department of Health and Human Services, nor does mention of trade names, commercial products, or organizations imply endorsement by the U.S. government.

27 September 1989; accepted 20 October 1989

Structural Basis for Misaminoacylation by Mutant *E. coli* Glutaminyl-tRNA Synthetase Enzymes

JOHN J. PERONA, ROBERT N. SWANSON,* MARK A. ROULD, THOMAS A. STEITZ, DIETER SÖLL

A single-site mutant of *Escherichia coli* glutaminyl-synthetase (D235N, GlnRS7) that incorrectly acylates in vivo the amber suppressor *supF* tyrosine transfer RNA ($tRNA^{Tyr}$) with glutamine has been described. Two additional mutant forms of the enzyme showing this misacylation property have now been isolated in vivo (D235G, GlnRS10; I129T, GlnRS15). All three mischarging mutant enzymes still retain a certain degree of tRNA specificity; in vivo they acylate *supE* glutaminyl tRNA ($tRNA^{Gln}$) and *supF* $tRNA^{Tyr}$ but not a number of other suppressor tRNA's. These genetic experiments define two positions in GlnRS where amino acid substitution results in a relaxed specificity of tRNA discrimination. The crystal structure of the GlnRS:$tRNA^{Gln}$ complex provides a structural basis for interpreting these data. In the wild-type enzyme Asp^{235} makes sequence-specific hydrogen bonds through its side chain carboxylate group with base pair G3 · C70 in the minor groove of the acceptor stem of the tRNA. This observation implicates base pair 3 · 70 as one of the identity determinants of $tRNA^{Gln}$. Isoleucine 129 is positioned adjacent to the phosphate of nucleotide C74, which forms part of a hairpin structure adopted by the acceptor end of the complexed tRNA molecule. These results identify specific areas in the structure of the complex that are critical to accurate tRNA discrimination by GlnRS.

THE ACCURACY OF PROTEIN BIOSYNthesis in living cells depends critically on the acylation of transfer RNA (tRNA) molecules with the correct amino acid. Aminoacyl-tRNA synthetases, the enzymes catalyzing this reaction, have a high degree of specificity in discriminating among structurally similar tRNA molecules. The identification of the specific chemical groups responsible for the selectivity of interactions between tRNA and protein has been the focus of many studies in which various physical, biochemical, and genetic techniques were used (*1–5*). This has led (for some systems) to the partial identification of the set of nucleotides, known as identity elements, which serve to distinguish that set of isoacceptor RNA's specific to a given amino acid in vivo (*6*). The development of the technology required for the in vitro synthesis of any desired tRNA has allowed the identification of the nucleotides required for tRNA recognition by yeast phenylalanyl-tRNA synthetase (*7*). Genetic and biochemical studies have shown that some identity elements of glutaminyl tRNA ($tRNA^{Gln}$) are located at the acceptor end (nucleotides G73 and U1 · A72) (*3*) and in the anticodon (U35) (*2, 4*).

Department of Molecular Biophysics and Biochemistry, and the Howard Hughes Medical Institute, Yale University, New Haven, CT 06511.

*Present address: Service de Biochimie, CNRS de Saclay, Saclay, France.

Table 1. Suppression of the $lacZ_{1000}$ gene by different amber suppressor tRNAs (see text). Lysates of λ phages carrying the *glnS*$^+$, *glnS7*, *glnS10*, and *glnS15* alleles were spotted onto lactose minimal plates seeded with $lacZ_{1000}$ strains carrying the various amber suppressors. The plates were examined for growth after 2 to 3 days of incubation at 30°C. Bacterial growth (+) indicates mischarging of the suppressor tRNA with glutamine. The nomenclature for the in vitro derived Cys, Phe, and Ala suppressors is according to (*6*).

Suppressor	*glnS* allele			
	glnS$^+$	*glnS7*	*glnS10*	*glnS15*
supD (Ser)	−	−	−	−
supE (Gln)	+	+	+	+
supF (Tyr)	−	+	+	+
supP (Leu)	−	−	−	−
pGFIB:Cys	−	−	−	−
pGFIB:Phe	−	−	−	−
pGFIB:Ala2	−	−	−	−

There has been considerably less progress, however, in discovering which amino acids in synthetases are crucial for recognition of their respective tRNA's (*8*). In order to address this question we have used an in vivo genetic approach to generate mutations in *glnS* (the gene for *E. coli* GlnRS), which cause misacylation of noncognate tRNA species with glutamine. Selection for mutants of GlnRS that can mischarge noncognate tRNA's with glutamine is based on the suppression spectrum of an amber mutation in the gene for *E. coli* β-galactosidase (the $lacZ_{1000}$ mutation). If not suppressed by a suppressor tRNA this mutant gene gives rise to a truncated β-galactosidase protein. Insertion of an amino acid in response to the amber codon gives rise to full-length protein. Thus, suppression with the glutamine-inserting *supE* tRNA allows cells to grow on minimal lactose plates. However, the serine-